A&A 403, 955–974 (2003)
DOI: 10.1051/0004-6361:20030416


Astronomy & Astrophysics

# Explanatory supplement of the ISOGAL-DENIS Point Source Catalogue⋆,⋆⋆

F. Schuller[1], S. Ganesh[2,1], M. Messineo[3], A. Moneti[1], J. A. D. L. Blommaert[4], C. Alard[1,5], B. Aracil[1], M.-A. Miville-Deschênes[6], A. Omont[1], M. Schultheis[1], G. Simon[5], A. Soive[1], and L. Testi[7]

[1] Institut d'Astrophysique de Paris, CNRS, 98 bis Bd Arago, 75014 Paris, France
[2] Physical Research Laboratory, Navarangpura, Ahmedabad 380009, India
[3] Leiden Observatory, University of Leiden, PO Box 9513, 2300 RA Leiden, The Netherlands
[4] Instituut voor Sterrenkunde, KU Leuven, Celestijnenlaan 200 B, 3001 Leuven, Belgium
[5] GEPI, Observatoire de Paris, 61 Av. de l'Observatoire, 75014 Paris, France
[6] Laboratoire de radioastronomie millimétrique, École Normale Supérieure & Observatoire de Paris, France
[7] Osservatorio Astrofisico di Arcetri, Largo E. Fermi, 5, 50125 Firenze, Italy

Received 20 August 2002 / Accepted 13 March 2003

**Abstract.** We present version 1.0 of the ISOGAL–DENIS Point Source Catalogue (PSC), containing more than 100 000 point sources detected at 7 and/or 15 $\mu$m in the ISOGAL survey of the inner Galaxy with the ISOCAM instrument on board the *Infrared Space Observatory* (ISO). These sources are cross-identified, wherever possible, with near-infrared (0.8–2.2 $\mu$m) data from the *DENIS* survey. The overall surface covered by the ISOGAL survey is about 16 square degrees, mostly (95%) distributed near the Galactic plane ($|b| \lesssim 1°$), where the source extraction can become confusion limited and perturbed by the high background emission. Therefore, special care has been taken aimed at limiting the photometric error to ∼0.2 mag down to a sensitivity limit of typically 10 mJy. The present paper gives a complete description of the entries and the information which can be found in this catalogue, as well as a detailed discussion of the data processing and the quality checks which have been completed. The catalogue is available at the Centre de Données Astronomiques de Strasbourg (via anonymous ftp to `cdsarc.u-strasbg.fr (130.79.128.5)` or via `http://cdsweb.u-strasbg.fr/cgi-bin/qcat?J/A+A/403/955`) and also via the server at the Institut d'Astrophysique de Paris (`http://www-isogal.iap.fr/`). A more complete version of this paper, including a detailed description of the data processing, is available in electronic form through the ADS service and at `http://www.edpsciences.org`.

**Key words.** catalogs – stars: circumstellar matter – Galaxy: bulge – Galaxy: disk – Galaxy: stellar content – infrared: stars

## 1. Introduction

The ISOGAL survey is the most sensitive mid-infrared wide-field survey dedicated to the inner Galaxy (see the accompanying paper Omont et al. 2003 and references therein for a review of its scientific goals and results). The large amount of ISO observations collected, in combination with the near-infrared data of the DENIS survey, has resulted in the production of a catalogue of $10^5$ point sources, the PSC. The first scientific results obtained include studies of the Galactic structure, analysis of the stellar populations comprising completely detected AGB stars with their mass-loss in particular fields (Pérault et al. 1996; Omont et al. 1999; Glass et al. 1999; Ojha et al. 2003), characterisation of interstellar extinction (Jiang et al. 2003), of infrared dark clouds (Hennebelle et al. 2001), and of young stellar objects (Felli et al. 2000, 2002; Schuller 2002).

A total of ∼16 square degrees of the inner Galactic disk ($|b| \lesssim 1°$) were observed, with strong emphasis on the inner Galactic bulge, at wavelengths of 7 and 15 $\mu$m, with a pixel scale of usually 6″ and sometimes 3″, down to a sensitivity limit of typically 10 mJy. A total of ∼250 hours of ISO time were used, making ISOGAL one of the largest programs performed by ISO. For the southern sky the results were combined with the $I$, $J$, $K_s$ (effective wavelengths equal to 0.79, 1.22 and 2.14 $\mu$m) ground-based data from the DENIS survey (Epchtein et al. 1994, 1997) in order to produce an (up to) 5-wavelength catalogue of point sources. Given the emphasis of ISOGAL on the inner Galactic regions, the DENIS coverage is available for 95% of the fields surveyed with ISOCAM.

As a comparison, the IRAS satellite, which made a breakthrough in the infrared window in 1983, performed an all sky survey resulting in a $2.5 \times 10^5$ point source catalogue, with a typical sensitivity (or 90% completeness level) around 0.5 Jy in low source density regions and at the shortest wavelengths. The four IRAS bands were centred at 12, 25, 60 and 100 $\mu$m,

*Send offprint requests to*: F. Schuller, e-mail: `schuller@iap.fr`

⋆ This is paper No. 18 in a refereed journal based on data from the ISOGAL project.

⋆⋆ Based on observations with ISO, an ESA project with instruments funded by ESA Member States (especially the PI countries: France, Germany, the Netherlands and the UK) and with the participation of ISAS and NASA; and on DENIS observations collected at the European Southern Observatory, Chile.

thus covering the mid- to far-infrared range, with a spatial resolution ranging from less than 1′ at 12 $\mu$m to about 4′ at 100 $\mu$m. The sensitivity of ISOCAM is about two orders of magnitude better than that provided by the IRAS detectors at 12 $\mu$m in the high source density regions (thus in particular in the Galactic plane). Indeed, as explained in the IRAS Explanatory Supplement (Sect. VIII), the typical 50% completeness limit flux density was about 1 Jy at 12 and 25 $\mu$m in the Galactic Plane, and even brighter at longer wavelengths.

More recently, the MSX (Midcourse Space Experiment, see Mill et al. 1994 for an overview) mission surveyed the complete Galactic Disk in the range $|b| \leq 5^\circ$ in the mid-infrared, using a 33 cm aperture telescope called SPIRIT III (Price et al. 2001). Six bands between 4 and 25 $\mu$m were surveyed simultaneously at a spatial resolution of ∼18″. The most sensitive band was the *A* band, centred at 8.3 $\mu$m, for which the present point source sensitivity limit is about 0.1 Jy. The survey of the Galactic Plane has presently resulted in a catalogue of $3.2\times10^5$ sources (Price et al. 2001), which permits a complete analysis of the most luminous infrared Galactic populations. The images of this survey have also led to the detection of more than 2000 infrared dark clouds (Egan et al. 1998). A very recent analysis (Lumsden et al. 2002) of the MSX PSC has produced a large sample of massive young stellar objects in the Galactic disk.

Among the many large observing programs conducted by ISO, including deep and wide-field extragalactic surveys, worth mentioning are the European Large-Area ISO Survey, ELAIS (Rowan-Robinson et al. 1999), ISOCAM deep surveys using guaranteed time observations (Elbaz et al. 1999), and FIRBACK, a deep 170 $\mu$m imaging survey carried out with ISOPHOT (Dole et al. 2001). Apart from these there were also a number of observations of specific targets in the Galaxy. The following ISOCAM studies were with sensitivities comparable to or slightly deeper than ISOGAL (in more limited areas): LW2 and LW3 imaging surveys of nearby star forming regions (Nordh et al. 1998; Bontemps et al. 2001), photometric studies of other Galactic HII regions (Zavagno & Ducci 2001), and the GPSURVEY (Burgdorf et al. 2000), which provided observations of about 0.25 deg$^2$ in the central Galaxy at mid-infrared wavelengths.

In this paper, we give a detailed description of the ISOGAL observations in Sect. 2, and of their processing and the related quality checks in Sect. 3. The DENIS data are presented in Sect. 4. The content of the Point Source Catalogue (PSC) is explained in Sect. 5, and the complete descriptions of various support tables are given in the relevant sections. Finally, the main characteristics of the catalogue are briefly summarised in Sect. 8.

## 2. ISOGAL observations and fields

### 2.1. ISOGAL observations

The mid-infrared observations were obtained with the ISOCAM instrument (Cesarsky et al. 1996; Blommaert et al. 2001) on ISO (Kessler et al. 1996) using filters centred at $\lambda \approx 7$ and 15 $\mu$m and with a pixel scale of 6″, or 3″ in a few cases.

**Table 1.** ISOCAM filters used for ISOGAL: reference wavelengths and bandwidths, zero point magnitudes and flux densities, and total observed area.

| Filter | $\lambda_{\rm ref}$ [$\mu$m] | $\Delta\lambda$ [$\mu$m] | $ZP^a$ [mag] | $F_{mag=0}$ [Jy] | Area [deg$^2$] |
|---|---|---|---|---|---|
| LW2 | 6.7 | 3.5 | 12.39 | 90.36 | 9.17 |
| LW5 | 6.8 | 0.5 | 12.28 | 81.66 | 0.64 |
| LW6 | 7.7 | 1.5 | 12.02 | 64.27 | 2.97 |
| LW3 | 14.3 | 6.0 | 10.74 | 19.77 | 9.92 |
| LW9 | 14.9 | 2.0 | 10.62 | 17.70 | 3.53 |

[a] The magnitude of a source with a flux density $F_\nu$ expressed in mJy is given by $mag = ZP - 2.5 \times \log(F_\nu)$.

Table 1 lists the filters used. Most observations were performed with the broad filters LW2 and LW3, with a field selection avoiding bright IRAS sources susceptible to detector array saturation. However, a few regions with stronger sources (around the Galactic Centre and in a few star forming regions) were observed with the narrow filters LW5 or LW6, and LW9, and with smaller pixel field of view (3″).

For standard ISOGAL observations (broad filters LW2 and LW3), we estimated that, to avoid saturation of the detector, no IRAS source with $F_{12\ \mu\rm m} \geq 6$ Jy should be observed. This limit was further relaxed up to $F_{12\ \mu\rm m} < 20$ Jy with narrow filters; however, even with such a high limit value, it implied that a few regions, including the Galactic Centre itself, could not be observed. A quick inspection of the images showed that only very few observed pixels among all ISOGAL observations were slightly above the limit of the linear domain of the detector. The profiles of the associated point sources do not deviate much from the average point spread function (PSF, see Sect. 3.2.1), so that no source suffers strongly from saturation in the published point source catalogue.

The observations were performed as rasters. The basic ISOCAM observation is a $32 \times 32$ pixel image of 0.28 s integration time. Due to limitations in the downlink data rate, these basic images were coadded in groups of four and downlinked, making the unit frame one of 1.12 s integration time. At each raster position 19 such frames were obtained, resulting in an integration time of ∼21 s per raster position. The rasters were oriented along galactic latitude and longitude, which differed from the direction of the sides of the detector array, resulting in "saw-tooth" edges of the final mosaics. With 6″ pixels, the raster steps were typically 90″ in one direction and 150″ in the perpendicular one (and a factor of two smaller with 3″ pixels), in order to observe each sky position about twice. However, because of the non-alignment of the raster and detector axes, each sky position was not as regularly observed. The actual number of observations per sky point varied from four to exceptionally zero (for the dead ISOCAM column close to a raster edge), with an average of ∼1.5.

The total area covered by the ISOGAL survey is ∼15.6 square degrees, of which 10.7 were observed at both 7 and 15 $\mu$m, 2.1 were observed at 7 $\mu$m only, and 2.8 were observed at 15 $\mu$m only. This survey is the result of three successive proposals developed over the lifetime of ISO. As a consequence, most fields were observed at 7 and

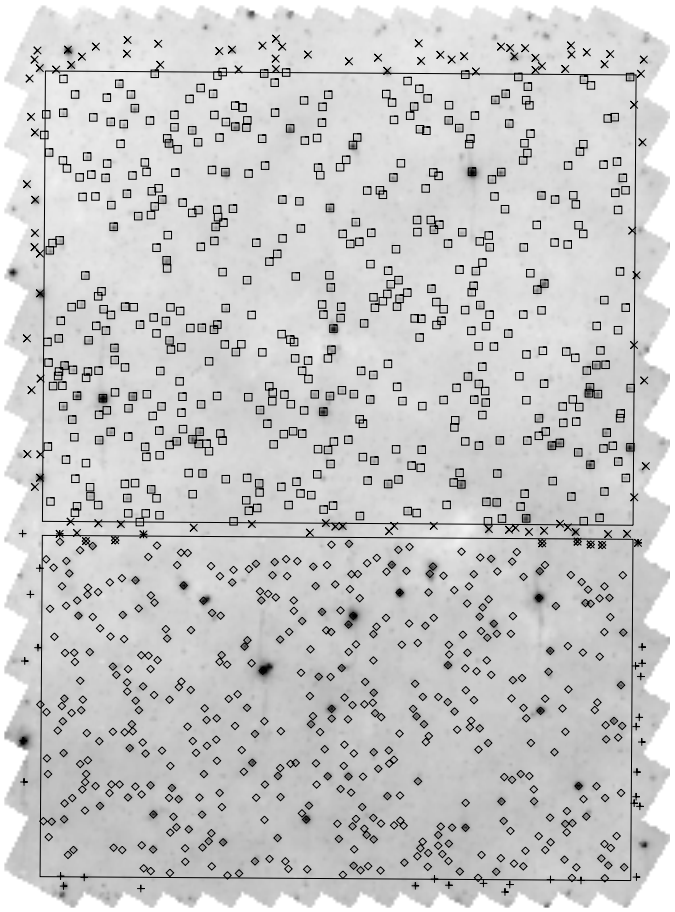

**Fig. 1.** Example of one ISOGAL observation which has been used for one FA and one FC fields. The formal limits of both fields are shown with rectangular frames: FC field (upper frame) and FA field (lower frame). The different symbols correspond to the different catalogues of sources (see Sect. 5): squares (FC, regular), crosses (FC, edge), diamonds (FA, regular) and plus signs (FA, edge).

15 $\mu$m at different dates, and some fields were observed at one wavelength only, in particular because the planned targets were not observable at the very end of the mission.

A total of 696 observations compose the ISOGAL survey. Of all these observations, 29 could not be used because of instrument failures or other problems during the data reduction. Another 18 observations are single ISOCAM frames ($32 \times 32$ pixels) observed in the spectroscopic *Circular Variable Filter* (CVF) mode; they are treated in a different way (Blommaert et al., in preparation). A further 186 images are "dummy" observations, containing only one $32 \times 32$ pixel image – acquired after repositioning of the telescope to allow for reconfiguring the camera from the CAM parallel mode to that of the observation – and have not been used for the catalogue. As a result, only 463 raster-observations are considered as relevant for the imaging survey.

To avoid redundancy in the published catalogue (due e.g. to various observations of a test field with several filters, but also to small overlapping areas between two observations in many cases), we decided to use, for the present version of the PSC, only one observation at 7 $\mu$m and one at 15 $\mu$m for a given position[1]. Thus, we had to choose the best observation in the case of overlapping images at the same wavelength. The selection criteria were: first, if the different observations are obviously of different quality, the best quality one was selected. Then, if the observations were made with different filters, we chose to keep the one with a broad filter (if it exists) because the number of detected sources is larger. In the very few cases where the filter is the same but the pixel size is different, we selected the large (6″) pixel observations in order to have more homogeneous data. If the quality and the observational setup were approximately the same in different observations, we then selected the most recent one (the one with higher ISO observation number), because on average the data quality was better certified. Finally, 384 raster images have been used to build the PSC.

All the raster images used are published with the PSC (and available through the CDS and IAP web sites[2]), and the electronic version of the catalogue of ISOGAL observations of the PSC contains 384 entries, each entry having the format described in Table 2. Two examples are shown in Table 3, for the 7 and 15 $\mu$m observations composing a test field of 0.027 deg$^2$ centred at $(l, b) = (0.0, 1.0)$, hereafter called the "C32" field.

### 2.2. Definition and list of "Catalogue Fields"

We define an ISOGAL "field" as a rectangular area of the sky whose edges are aligned with the galactic axes, and which has been completely observed with ISOCAM. There are three kinds of fields, depending on the available observations: the "FA" fields were observed only at 7 $\mu$m, the "FB" fields were observed only at 15 $\mu$m, and the "FC" fields were observed at both 7 $\mu$m and 15 $\mu$m.

To build the present version of the PSC, we have defined a total of 43 FA fields, 57 FB fields and 163 FC fields. In some cases, a fraction of an ISOGAL observation was used for an FA (or FB) field, and another fraction was used for an FC field (see e.g. Fig. 1), so that only 384 different observations were required for these 263 fields. These peculiar configurations can result in the presence of a few redundant sources: because of edge effects, two sources at the same position may appear in two different catalogues; nine such cases can be seen in Fig. 1 (see also Sect. 5.1). The complete catalogue of the 263 ISOGAL fields is available electronically[3] and contains 18 columns, as described in Table 4, and an example is given in Table 5.

The field names are generated using 14 characters, and the first two indicate the type of the field (FA, FB or FC). The 12 last characters of the field names are the galactic coordinates in decimal degrees of the centre of the field. A graphical view of the observed fields is given in Fig. 2.

[1] However, in very few cases due to edge effects, two ISOGAL sources have exactly the same final coordinates because they are associated with the same DENIS source (see also Sect. 5.1).

[2] `http://www-isogal.iap.fr/Fields/index_tdt.html`

[3] `http://www-isogal.iap.fr/Fields/` and at the CDS: `http://cdsweb.u-strasbg.fr/cgi-bin/qcat?J/A+A/403/955`

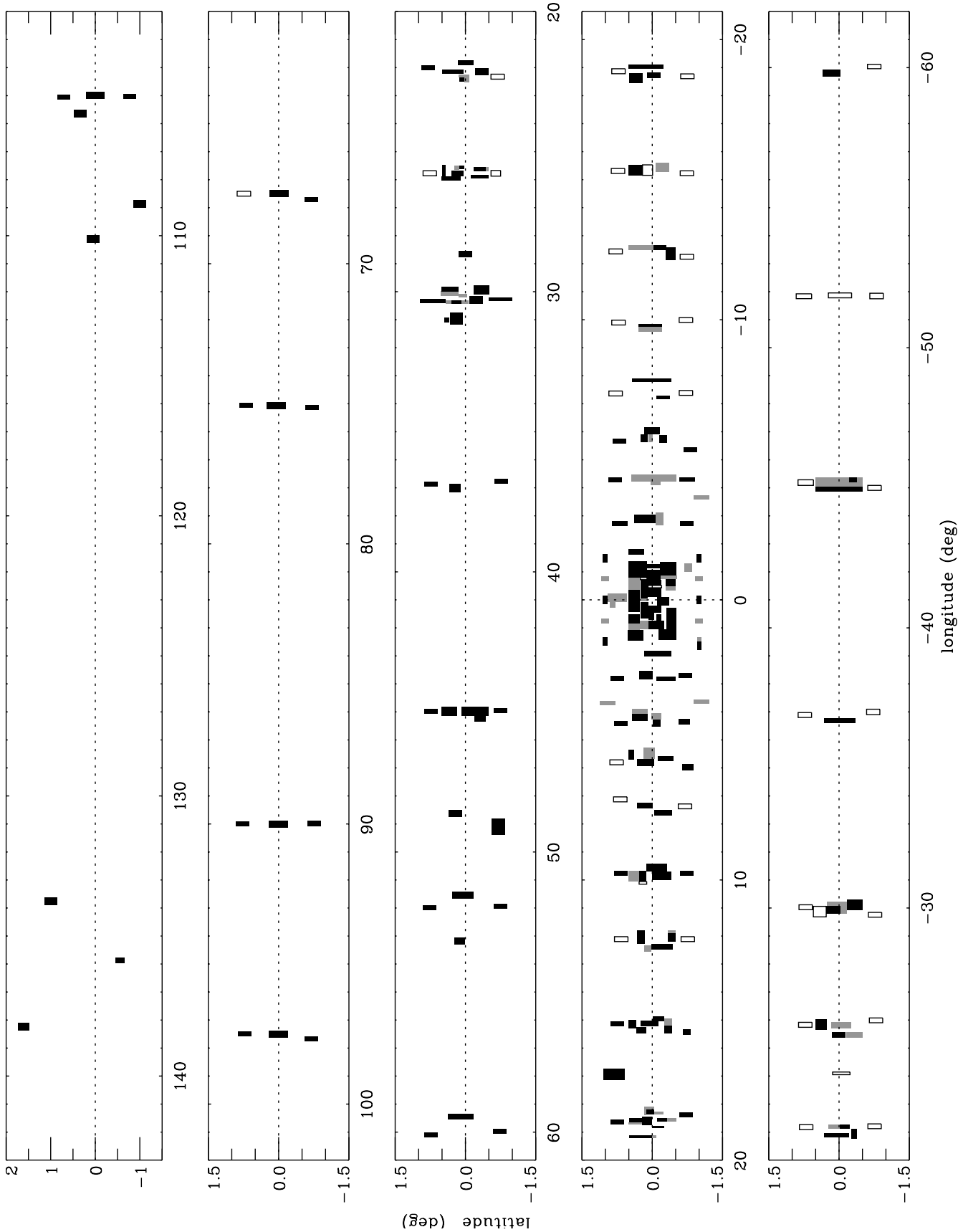


**Fig. 2.** Galactic map of the ISOGAL disk fields. The black boxes show the fields which have been observed at both 7 and 15 $\mu$m (FC fields), while the open boxes stand for 7 $\mu$m only observations (FA), and the grey ones for 15 $\mu$m only observations (FB).

**Table 2.** Format of ISOGAL observations Table (version 1) – 384 entries (see examples in Table 3).

| Col. | Name | Format | Units [range] | Description |
|---|---|---|---|---|
| 1 | ION | a8 | | ISO Observation number |
| 2 | name | a13 | | ISOGAL observation name |
| 3 | date | a6 | YYMMDD | date of observation |
| 4 | j_day | i4 | | Julian day of observation - 2 450 000 |
| 5 | qual | i1 | [1,2] | quality of image[a] |
| 6 | *l*_off | f5.1 | arcsec | applied offset in Galactic longitude[b] |
| 7 | *b*_off | f5.1 | arcsec | applied offset in Galactic latitude |
| 8 | G_lon | f8.4 | deg [−180–+180] | Galactic longitude of raster centre |
| 9 | G_lat | f8.4 | deg [−90–+90] | Galactic latitude of raster centre |
| 10 | *dl* | f6.4 | deg | half width of raster in longitude |
| 11 | *db* | f6.4 | deg | half width of raster in latitude |
| 12 | RA | f8.4 | deg | RA (J2000) of raster centre |
| 13 | DEC | f8.4 | deg | Dec (J2000) of raster centre |
| 14 | filt | i1 | [2,3,5,6,9] | LW filter number |
| 15 | pfov | i1 | arcsec [3,6] | pixel field of view |
| 16 | mag_lim | f5.2 | mag | ISO magnitude cutoff[c] |
| 17 | nb_sour | i4 | | number of extracted sources brighter than mag_lim |
| 18 | rot | i1 | [0,1] | applied transformation (270° rotation) to the raster[d] |
| 19 | *x*_inv | i1 | [0,1] | applied transformation (*x*-inversion) to the raster |
| 20 | *y*_inv | i1 | [0,1] | applied transformation (*y*-inversion) to the raster |
| 21 | *m* | i2 | | number of raster steps in *x* in final raster |
| 22 | *n* | i2 | | number of raster steps in *y* in final raster |
| 23 | *dm* | i3 | arcsec | size of step between *x* (final) raster positions |
| 24 | *dn* | i3 | arcsec | size of step between *y* (final) raster positions |
| 25 | angle | f6.2 | deg | angle from the upward axis to the north in the final raster |
| 26 | *NX* | i3 | pixel | number of pixels in *x* of final raster |
| 27 | *NY* | i3 | pixel | number of pixels in *y* of final raster |

[a] Image quality: 1 is standard quality, 2 is medium quality (in most cases, the problem is that the first individual image of the raster appears brighter than the other ones). Images of bad quality have not been used to build the catalogue.
[b] The astrometry of the published raster images has been corrected to match the DENIS astrometry if any (see Sect. 7). The offset values given in this table have been added to the initial raster coordinates.
[c] The ISO magnitude cutoff has been computed for each observation to correspond at least approximately to a 50% completeness level (see Sect. 3.4).
[d] Columns 18–20: all the published images are oriented with *l* along decreasing *x* and *b* along increasing *y*. In each column, a 1 means that the corresponding transformation has been applied to the initial (OLP7 processed) raster, and a 0 means that this transformation was not needed.

**Table 3.** Two examples of entry in the ISOGAL observations Table (see Table 2 for explanation), from the "C32" field at $(l, b) = (0.0, 1.0)$.

| Col. | 1 | 2 | 3 | 4 | 5 | 6 | 7 | 8 | 9 | 10 | 11 | 12 |
|---|---|---|---|---|---|---|---|---|---|---|---|---|
| Name | ION | Name | date | j_day | qual | *l*_off | *b*_off | G_lon | G_lat | *dl* | *db* | RA |
| Ex. 1 | 83600418 | 2P00P10B | 980228 | 873 | 1 | −4.8 | −5.6 | 0.0001 | 0.9988 | 0.1633 | 0.0758 | 265.4353 |
| Ex. 2 | 83600523 | 3P00P10B | 980228 | 873 | 1 | −6.3 | −3.1 | −0.0003 | 0.9995 | 0.1633 | 0.0758 | 265.4353 |

| Col. | 13 | 14 | 15 | 16 | 17 | 18 | 19 | 20 | 21 | 22 | 23 | 24 | 25 | 26 | 27 |
|---|---|---|---|---|---|---|---|---|---|---|---|---|---|---|---|
| name | DEC | filt | pfov | mag_lim | nb_sour | rot | *x*_inv | *y*_inv | *m* | *n* | *dm* | *dn* | angle | *NX* | *NY* |
| Ex. 1 | −28.4136 | 2 | 6 | 8.89 | 331 | 1 | 0 | 0 | 7 | 4 | 150 | 90 | 58.95 | 196 | 91 |
| Ex. 2 | −28.4136 | 3 | 6 | 8.00 | 220 | 1 | 0 | 0 | 7 | 4 | 150 | 90 | 58.97 | 196 | 91 |

## 3. ISOGAL data processing and quality

A complete description of the data processing and of the procedures that were run to quantify the quality of the data is given in the electronic version of this paper, available through the ADS service[4]. Only the main results, which may be useful to all users of the catalogue, are summarised in this section and the following one.

[4] Or directly at `http://www.edpsciences.org`

### 3.1. ISOCAM image processing

Data reduction was performed with standard procedures of the CAM Interactive Analysis (CIA, Ott et al. 1997) package version 3.0 on data products produced with version 7.0 of the ISO Off-Line Processing (OLP) pipeline (Blommaert et al. 2001). A particular care was taken to correct the effect of the slow detector responsitivity. Two methods of transient correction were used: the IAS model transient correction (Abergel et al. 1998), also called the "inversion" method, was used to get the

**Table 4.** Format of ISOGAL "Fields" Table (version 1) – 263 entries (see example in Table 5).

| Col. | Name | Format | Units [range] | Description |
|---|---|---|---|---|
| 1 | Name | a14 | | ISOGAL field identifier |
| 2 | ION7 | a8 | | ION for 7 $\mu$m data (see Table 2) |
| 3 | ION15 | a8 | | ION for 15 $\mu$m data |
| 4 | filt7 | i1 | [2,5,6] | 7 $\mu$m filter |
| 5 | filt15 | i1 | [3,9] | 15 $\mu$m filter |
| 6 | pfov | i1 | arcsec [3,6] | pixel field of view |
| 7 | G_lon | f8.4 | deg [−180–+180] | Galactic longitude of field centre |
| 8 | G_lat | f8.4 | deg [−90–+90] | Galactic latitude of field centre |
| 9 | *dl* | f6.4 | deg | half width of field in longitude[a] |
| 10 | *db* | f6.4 | deg | half width of field in latitude[a] |
| 11 | area | f6.4 | deg$^2$ | area of field |
| 12 | dens7 | i5 | deg$^{-2}$ | density of 7 $\mu$m sources |
| 13 | dens15 | i5 | deg$^{-2}$ | density of 15 $\mu$m sources |
| 14 | RMS_II | f4.2 | arcsec | RMS separation of 7–15 $\mu$m associated sources |
| 15 | RMS_ID | f4.2 | arcsec | RMS separation of ISO-DENIS associated sources |
| 16 | $K$_max1 | f4.1 | mag | DENIS $K_s$ magnitude cutoff 1[b] |
| 17 | $K$_max2 | f4.1 | mag | DENIS $K_s$ magnitude cutoff 2[c] |
| 18 | dens_K2 | i5 | deg$^{-2}$ | density of DENIS $K_s$ sources used[d] |

[a] *dl* and *db* apply to the limits inside the edges of the images within which sources are accepted.
[b] maximum DENIS $K_s$ magnitude limiting the density of $K_s$ DENIS sources to ∼18 000 sources per square degree if the ISO images have 6″ pixels (or to ∼72 000 sources per square degree for the 3″ ISO observations). $K$_max1 is used to discuss the quality of ISOGAL–DENIS associations (see Sect. 4.3.4).
[c] maximum DENIS $K_s$ magnitude accepted in order to avoid spurious cross-identifications. The density of $K_s$ DENIS sources is limited to ∼36 000 sources per square degree for 6″ ISO observations (and again to ∼72 000 sources per square degree for 3″ ISO observations).
[d] density of DENIS $K_s$-band sources brighter than the cutoff magnitude $K$_max2.

**Table 5.** Example of entry in the ISOGAL fields table (Table 4) ("C32" field at $(l, b) = (0.0, 1.0)$).

| Col. | Name | C32 field |
|---|---|---|
| 1 | Name | FC+00000+00100 |
| 2 | ION7 | 83600418 |
| 3 | ION15 | 83600523 |
| 4 | filt7 | 2 |
| 5 | filt15 | 3 |
| 6 | pfov | 6 |
| 7 | G_lon | −0.0011 |
| 8 | G_lat | 0.9990 |
| 9 | *dl* | 0.1441 |
| 10 | *db* | 0.0471 |
| 11 | area | 0.0271 |
| 12 | dens7 | 9225 |
| 13 | dens15 | 6125 |
| 14 | RMS_II | 2.24 |
| 15 | RMS_ID | 1.70 |
| 16 | $K$_max1 | 9.6 |
| 17 | $K$_max2 | 10.6 |
| 18 | dens_K2 | 35979 |

best photometry for non-stabilised signals, while the auxiliary "vision" method (Starck 1998; Starck et al. 1998) was used to remove most of the latent images (or remnants) due to memory effects of the detectors to strong sources (Coulais & Abergel 2000). We thus have two sets of reduced data: a) the main one treated with "inversion", which performs a correction for the missing signal, (though this correction is not perfect, see Sect. 3.3), but which still contains the remnants; b) an auxiliary one, roughly treated with "vision", where most remnants have been removed, but with wrong photometry. The two rasters are converted to physical units (mJy), using the standard conversion factors (Blommaert 1998).

### *3.2. Point source extraction*

#### 3.2.1. The point source extraction procedure

A dedicated PSF fitting procedure worked out by C. Alard has been used to extract point sources from all "inversion" and "vision" processed images. First, a search for local maxima is performed on the complete image, resulting in a list of pixel positions of point source candidates. Then, an analytical expression of the PSF is fitted at each position to compute the flux density of the point sources, and to discard the local maxima whose shapes do not correspond to the instrumental response to a point source.

The source detection is first performed on an oversampled image, using pixels a factor of two smaller than in the initial image. This image is used only for the detection step of the source extraction. The oversampling is performed by a convolution of the initial pixels with an analytical expression of a theoretical PSF. As a result, the sources can be localised on a thinner grid.

The detection procedure looks for local maxima in the oversampled image. This step is controlled by a *mesh* parameter, which can take values of 1 or 2, and defines the size of the grid on which local maxima are looked for. With *mesh* = 1, all local maxima are detected, even those corresponding to bright spots

in the background rather than to point sources. On the other hand, with *mesh* = 2, 5 × 5 oversampled pixel meshes are used to find local maxima, resulting in a smoothing of the irregularities in the background, without any significant loss in the detection of relatively bright ($F_\nu \gtrsim 100$ mJy) point sources, but with a more confusion limited extraction of the faintest sources.

The extraction procedure which has been used to build the ISOGAL PSC performed a complete extraction with each value of *mesh*. For each observation, the two resulting catalogues have been cross associated to check the quality and the reality of the detected sources (see Sect. 3.2.2). Obviously the extraction performed with *mesh* = 1 is the most efficient to correctly extract blended sources; on the other hand, a non negligible fraction of the sources extracted only with *mesh* = 1 (with no association in the extraction performed with *mesh* = 2) seem to be spurious (see the discussion in Sect. 3.5.2).

Another procedure is used to measure the flux density of the sources on the original image, and to estimate the correlation of their profile with the PSF. For each observational setup (combination of one filter and one pixel scale), a single reference PSF has been determined for all the observations from a sample of relatively bright and isolated sources. A least square fit between the reference profile and a 5×5 (not oversampled) pixel mesh is computed at the position of each source candidate, starting with the brightest one. The background is estimated from the median value of the pixels in an annulus of inner and outer radii equal to 3 and 5 pixels, respectively. The results of this operation are the flux density of the source and the uncertainty on its measurement, computed as the RMS of the residual between the scaled PSF profile and the actual source profile. This flux density uncertainty is later converted to a magnitude uncertainty, hereafter called $\sigma$. The reality of each point source is estimated by the ratio of the fitted flux density to the RMS uncertainty of the fit, and only sources with this ratio greater than 3 are considered valid and stored in the resulting catalogue. Then, the profile of the source is subtracted from the image, and the procedure runs iteratively going to fainter and fainter sources. This method is powerful even in crowded fields, where it is able to estimate correctly the flux densities of blended sources.

### 3.2.2. Source quality checks

Four catalogues have been built for each observation, combining the two possible values of *mesh* (1 or 2) and the "inversion" and "vision" processed rasters. Considering the high background level in the Galactic Disk, we decided to anyhow limit the published catalogue to a flux density of 5 mJy ([7] ≈ 10.5 and [15] ≈ 9.0) to reduce the number of spurious sources (another limit was eventually later applied depending on the field, see Sect. 3.4). Then, the sources found in "inversion" processed images that were associated with a "vision" source within a search radius of one observed pixel were considered valid, while those found only in the "inversion" images were considered spurious (these can be remnants of bright sources, or other non real point-like sources). The distance between the "inversion" and the "vision" sources gives a good estimate of the quality of the sources: it is generally smaller than 1″ for real sources, while a separation larger than 3″ may be due to artifacts (see also Sect. 3.2.5). The final data (position and photometry) in the catalogue come only from the "inversion" processed rasters, with elimination of the remnant sources using the "vision" results.

The majority (70%) of the extracted sources could be associated between the *mesh* = 1 and the *mesh* = 2 catalogues (with a 6″ association radius for all observations), while the remaining 30% are only found with *mesh* = 1. Since less than 1% of the extracted sources were detected with *mesh* = 2 with no counterpart in the *mesh* = 1 catalogue, while almost 30% of the extracted sources were only detected with *mesh* = 1, the published data (position and photometry) come from the *mesh* = 1 results for the sources which were detected with both values, in order to get a homogeneous set of data. Further quality selection criteria are applied later in the processing (see Sect. 3.2.5), so that only ≈10% of the sources in the published catalogue have been detected with *mesh* = 1 only. A special MESH flag is included in the catalogue to indicate for which value(s) of *mesh* a source has been extracted, and the global QUALITY flag is decreased for sources without association between the *mesh* = 1 and the *mesh* = 2 results (see next section).

### 3.2.3. Source extraction quality flags

The quality of the derived photometry as well as the reliability of the extracted sources can be affected by several factors, and different quality flags have been computed to warn the user when effects degrading the photometric quality are present, and to finally estimate the global quality of the point sources.

#### The MESH flag

The *MESH* flag is set to 1 (resp. 2) for sources which have been detected only with *mesh* = 1 (resp. 2), and to 3 for the sources which could be associated between the two extractions (see Sect. 3.2.2), thus making their reality more trustful.

#### The NPIX flag

The number of independent measurements of the signal at the position of a source, which takes into account the number of coadded individual exposures, but also the fact that some exposures might be discarded due to glitches or to the ISOCAM dead column, directly affects the photometric quality. The NPIX flag is the integer part of one tenth of the weighted number of measurements usable at the central position of the source, as given in the third plane of the OLP7 processed FITS files. As each raster position has been observed on average 19 × 1.5 (see Sect. 2.1) times, typical "good quality" values of this flag are in the range 2 to 4. Note that this flag is rather an indication of the number of good exposures than a number of pixels involved, but we decided to keep the NPIX name, as it appears in the header of the OLP7 processed files.

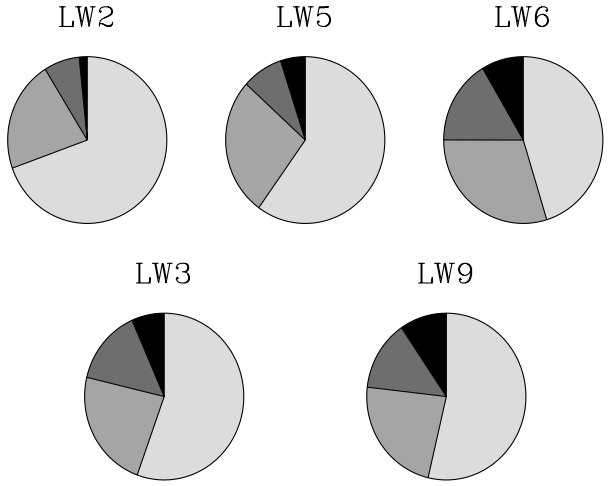


**Fig. 3.** Distribution of the quality flag $Q$ for the different filters. The gray scale corresponds to the different values of this flag, from 4 (lightest grey) to 1 (darkest grey).

#### The EDGE flag

The position of a source with respect to the edges of the raster also affects the derived photometric quality, because the extraction procedure needs a large enough observed area to properly compute the flux density of the source and the background to be subtracted. The EDGE flag is set to 1 when the centre of the source is at a distance between two and five pixels from the edge of the observed raster (taking into account the saw-tooth borders), and to 0 when the distance is greater than five pixels. Sources at less than two pixels from one edge were removed from the catalogue, since their flux density cannot be properly estimated.

#### The global quality flag $Q$

A global quality flag $Q$ was computed by combining the flags defined above and the photometric uncertainty $\sigma$. Its value ranges from 1 to 3 for sources with $MESH = 1$ or 2, and from 2 to 4 for sources with $MESH = 3$, the higher the better quality. The distribution of this flag for all the sources in the catalogue is shown for the different filters in Fig. 3. As can be seen, more than one half of the sources have a very good photometric quality ($Q = 4$). A value of 3 for this flag can also be considered as reasonably good quality. Finally, only ~15% of the sources in the catalogue have a moderate photometric quality ($Q \leq 2$). They should be used with much caution since their reliability is not warranted.

Additional estimates of the reliability of the sources are provided by the analysis of repeated or overlapping observations (see Sect. 3.5.1), but also by the combination of several wavelengths, including DENIS ones: a source with a moderate quality flag at, for example, 7 $\mu$m, but with a good quality association at 15 $\mu$m (see Sect. 3.6) finally has a very large probability to be a real source.

#### 3.2.4. Extended sources

The first version of the ISOGAL PSC only contains point sources, and sources of very small extension. The extraction of extended objects will be performed with a dedicated procedure for the second version of the catalogue.

The present version of the PSC contains a small proportion of sources of small extension, with typical sizes around 10–20″ (FWHM). These slightly-extended sources are characterised by relatively high values of the photometric uncertainty, with typical $\sigma \approx 0.15$ mag for bright ($F_\nu \approx 1$ Jy) sources, while bright point sources generally have $\sigma < 0.05$ mag. Aperture photometry performed on a small sample of such bright slightly extended sources has shown that their magnitudes can be underestimated by about 1 mag (Schuller 2002). It is planned to perform accurate photometry and to include a relevant extension flag in the second version of the PSC.

#### 3.2.5. Spurious sources

Three kinds of extracted sources are considered as spurious: (1) the "inversion-only" sources, i.e. those found in "inversion" rasters with no counterpart in the "vision" rasters, (see Sect. 3.2.2), (2) the sources with an inversion-vision association with a large separation (≥0.5 pixel) and with a poor extraction confirmation (flag $MESH < 3$), and (3) the other possible remnants of bright sources. Indeed, the "vision" method (see Sect. 3.1) does not remove all remnant sources, and remaining remnants of bright (≥100 mJy) sources were identified by looking for faint sources within a radius of 0.5 pixel around the exact location of the bright source in the detector at the five successive positions in the raster. They have been removed from the catalogue and their positions and magnitudes are listed in the catalogue of spurious sources (Sect. 6). Unfortunately, true faint sources which are found at the position of a putative remnant are also considered as spurious, and appear in the catalogue of spurious sources but not in the PSC.

### *3.3. Photometric calibration*

The flux densities of the point sources, as obtained by the PSF fitting procedure, lead to a good relative photometry, but have to be calibrated in an absolute way. Two factors introduce biases in the photometry. First, the integration time for the standard ISOGAL observations was too short to allow the signal to stabilise. A correction to this transient problem is applied with the "inversion" method (see Sect. 3.1). However, this method only allows proper correction for extended emission, but is insufficient for point sources (Coulais & Abergel 2000; Blommaert 1998). A few ISOGAL fields were observed with longer integration times. A comparison between *regular* and *long* measurements showed that the photometry from the *regular* raster is about 0.2 mag too high (too faint).

Our PSF photometry introduces a second bias, because a fraction of the signal from a point source falls outside the mesh used to model the PSF. The general flux calibration of ISOCAM was established from measurements on standard stars (Blommaert 1998; Blommaert et al. 2000). The observed

signal was measured using aperture photometry, which was corrected for the part of the PSF falling outside the aperture. To convert our PSF-fitting photometry to absolute photometry, a comparison was made with photometry obtained using the same techniques as in the ISOCAM general flux calibration. The aperture magnitudes were found to be lower (brighter) than the PSF magnitudes by 0.2–0.4 mag, revealing a bias in the PSF normalisation.

#### 3.3.1. Final correction

The total correction that has to be applied is between −0.37 and −0.59 mag for the different setups. As the uncertainty on each determined correction is at least 0.1 mag we decided to apply the same constant offset of −0.45 mag to all the sources and for all observational setups. This correction leads to photometry in good agreement with external comparison data, as is explained below.

The first publications based on ISOGAL data made use of a non-corrected photometry. The mid-infrared magnitudes presented there should thus be corrected by a −0.45 mag offset (with a possible ±0.1 mag additional discrepancy from field to field). This concerns in particular the results published in Pérault et al. (1996), Testi et al. (1997), Omont et al. (1999), Glass et al. (1999), Schultheis et al. (2000) and Felli et al. (2000). Appropriate errata will be published for these papers.

#### 3.3.2. External checks

The comparison of the observed with the predicted photometry for stars with known spectral types and distances provides an absolute calibration. Comparing the predicted and the corrected PSF magnitudes for three stars from the Hipparcos Input Catalogue we obtain:

$$mag_{\rm pred} - mag_{\rm PSF} = 0.04 \pm 0.10$$

where the result is the average of all determinations, independent of filter-PFOV combination, and the uncertainty is the variance of the six determinations obtained, though the distribution of these determinations is clearly non-Gaussian.

A second check on the photometry is provided by the cross calibration with the published catalogue of bright sources detected by the MSX survey of the Galactic Plane (Price et al. 2001). A comparison with the band *D* photometry of MSX, which used a filter similar to the ISOCAM 15 $\mu$m filters, showed good agreement between the corrected ISO magnitudes and the MSX ones. For 650 stars (424 observed with LW3 and 226 with LW9) we find:

$$mag_{\rm MSX} - mag_{\rm PSF} = 0.01 \pm 0.40$$

where the uncertainty is the RMS of the measured differences in magnitude. The large width of the distribution is due to the combination of the ISO and MSX photometry uncertainties, and to the intrinsic variability of many of such bright stars. Note that, strictly speaking, this result is valid for the brightest ISOGAL stars that could also be measured by MSX (which means roughly $[15] \lesssim 4.0$). Moreover, the computation of the mean difference in magnitudes was limited to an even brighter sample ($[15] < 3.0$) in order to avoid Malmquist bias. This nevertheless shows that our photometric calibration is reasonably good and in agreement with others.

### 3.4. Artificial sources

Artificial star experiments (see Bellazzini et al. 2002 and references therein for a general description) were conducted on the ISOGAL images in order to study the effects of a crowded field on the photometric quality and the completeness of the extracted point source catalogue. A procedure was created for adding artificial stars to the ISOGAL images, for extracting the sources with the same pipeline as the one used to generate the ISOGAL catalogue, and for checking how well the input sources are extracted.

Artificial star experiments enabled us to evaluate both random and systematic photometric errors due to crowding, as well as the completeness level of the extraction. The output magnitudes were found brighter than the input ones. This bias is very small for bright stars, but can reach 0.3 mag for the faintest ones in the densest fields, where the probability of blending with real stars is higher (see e.g. Fig. E-10 in the electronic version of this paper).

The completeness of the extraction can be quantified as follows. For each observation, we can plot the fraction of simulated sources which were retrieved as a function of input magnitude. We observe a smooth curve which drops for the faintest magnitudes. The magnitude where this fraction becomes less than 50% strongly depends on the density of the field. We used this trend to define the limiting magnitudes for each observation, corresponding to the faintest sources that were included in the published catalogue. These magnitudes are generally consistent with the magnitudes above which the bias reaches 0.1 mag and its standard deviation reaches 0.3 mag. We derived relations between source density and limiting magnitudes for the different observational setups (see also Figs. E-13 and E-14 in the electronic version). We make a distinction between the core of the ISOGAL survey observed with broad filters and 6″ pixels and the peculiar observations of difficult fields observed with narrow filters and 6″ or 3″ pixels.

#### A) 6″ pixel observations with broad filters

For the 6″ pixel observations with LW2 and LW3 filters, we computed the following linear relations:

– for LW2 observations:

$$mag_{\rm lim} = \begin{cases} 10.1 & \text{if } d \le 0.01, \\ 10.7 - 60. \times d & \text{if } d \ge 0.01, \end{cases} \quad (1)$$

where $d$ is the source density expressed in source/pixel. Thus, the limiting magnitude ranges from 10.1 to 8.8, corresponding to limiting flux densities between 8 and 27 mJy.

– for LW3 observations:

$$mag_{\rm lim} = \begin{cases} 8.7 & \text{if } d \le 0.005, \\ 8.9 - 40. \times d & \text{if } d \ge 0.005. \end{cases} \quad (2)$$

**Table 6.** Limiting magnitudes used to cut the catalogues for 3″ pixel observations.

| Filter | LW2 | LW5 | LW3 | LW9 |
|---|---|---|---|---|
| $mag_{\rm lim}$ | 10.0 | 8.4 | 8.5 | 7.0 |

Here, the limiting magnitude ranges from 8.7 to 7.7, and the associated flux density ranges from 6.5 to 16 mJy.

### B) 6” pixel observations with narrow filters

The results of our artificial source simulations show that the completeness level is generally worse in LW5, LW6 and LW9 observations, which can be interpreted as an effect of the much brighter diffuse background in the peculiar regions which needed the use of such narrow filters. Therefore, we applied 0.5 mag brighter cutting criteria for the 6″ observations with these filters:

– for LW5 and LW6 observations:

$$mag_{\rm lim} = \begin{cases} 9.6 & \text{if } d \leq 0.01, \\ 10.2 - 60. \times d & \text{if } d \geq 0.01, \end{cases} \quad (3)$$

– for LW9 observations:

$$mag_{\rm lim} = \begin{cases} 8.2 & \text{if } d \leq 0.005, \\ 8.4 - 40. \times d & \text{if } d \geq 0.005. \end{cases} \quad (4)$$

In addition, the photometry of the faintest sources in these peculiar fields is less accurate than in standard observations. Therefore we decided to decrease the quality flags (see Sect. 3.2.3) for the sources with magnitudes between $mag_{\rm lim}$-0.5 and $mag_{\rm lim}$, and we extended the range in which we decreased the quality flags down to $mag_{\rm lim}$-1 for the most difficult FC+01694+00081 field located in the M16 nebula.

### C) 3″ pixel observations

The situation is more complicated for the 3″ pixel observations, because they are too few and peculiar to allow a global statistical treatment. Artificial source simulations have been run on all the 3” pixel observations used in the PSC, and the results show good agreement between the different observations with a given filter. Therefore we used a single limiting magnitude for each filter, and the different values are given in Table 6. These limits give reasonably good results in terms of bias and completeness.

#### 3.4.1. Conclusion: limiting the Point Source Catalogue

The distribution of the limiting magnitudes, as defined in the previous section (Eqs. (1)–(4) for 6″ pixel observations, Table 6 for 3″ pixel observations) for all ISOGAL observations is shown in Fig. 4. Since most observations were done with the broad LW2 and LW3 filters, these histograms show that the typical reached sensitivity is around 20 mJy at 7 $\mu$m and 12 mJy at 15 $\mu$m.

When we apply these relations to all the ISOGAL catalogues, we eliminate ≈25% of the sources. This photometric cut is far more severe for moderate quality sources than for good quality ones: if we consider the *QUALITY* flag as defined in Sect. 3.2.3, it appears that about one half of the sources with *QUALITY* = 1 or 2 are discarded, while ∼30% of the sources with *QUALITY* = 3 and ∼12% of the sources with *QUALITY* = 4 are removed by this cut.

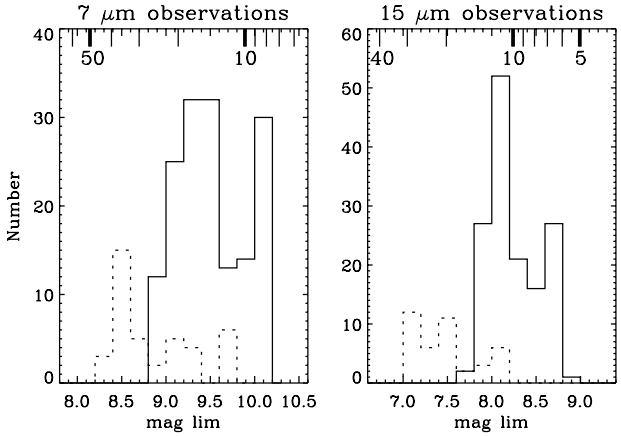


**Fig. 4.** Distribution of the magnitudes $\rm mag_{lim}$ at which the catalogues have been cut for the broad filters LW2 and LW3 (full lines), and for the narrow filters (dotted lines). However, note that, for the narrow filters, the data with magnitudes higher than $mag_{\rm lim}$-0.5 are of poor quality (see text, Sect. 3.4 B). The logarithmic scales at the top of each panel show the corresponding flux densities in mJy for LW2 and LW3. A small correction has to be applied for the corresponding flux densities with narrow filters (see Table 1).

## 3.5. Repeated observations

### 3.5.1. Overlapping 6″ observations

A few ISOGAL fields have been observed twice or more with exactly the same observational setup (filter and pixel size), and a large number of fields have overlapping regions. The total surface of such repeatedly observed areas is ∼0.7 deg$^2$. A comparison of the photometry extracted from such independent observations of the same regions of the sky was performed, and the main results for each observational setup are given in Table 7. Note that, because of the variability of some sources, the quoted standard deviations in Table 7 are slightly above the true photometric uncertainty of the final catalogue multiplied by $\sqrt{2}$.

It is also possible to get information about the completeness from the fraction of sources detected in both overlapping observations. It is however difficult to accurately estimate the completeness level by this method, as neither of the two catalogues is complete. It is nevertheless possible to have a rough estimate by comparing the catalogue extracted from a 6″ pixel observation with the more complete one, extracted from a 3″ pixel observation of the same region. Then we can compute the magnitude above which the fraction of 3″ sources found in the 6″ catalogue is below 50%. Taking into account all the limitations inherent to this method, the final results are essentially consistent with those derived from the artificial sources simulations, and also confirm that more care has to be taken for the observations performed with narrow filters.

**Table 7.** Main results of the comparison of repeated observations.

| Filter | Overlap surface ($deg^2$) | Nb. of sources | $\langle\Delta mag\rangle$ | *RMS* |
|---|---|---|---|---|
| LW2 | 0.166 | 2793 | 0.008 | 0.21 |
| LW6 | 0.098 | 1974 | 0.005 | 0.22 |
| LW3 | 0.275 | 2244 | 0.009 | 0.23 |
| LW9 | 0.111 | 1250 | 0.007 | 0.28 |
| Total | 0.650 | 8261 | 0.003 | 0.23 |

### 3.5.2. Reality of the extracted sources

An additional check of the reality of the sources can be performed as follows. The sources extracted from 6″ pixel observations should also be found in a 3″ pixel observation of the same region, because the sensitivity is generally greater in the latter, since the source extraction is much less limited by confusion. Also sources detected at one wavelength and with a good quality association at another ISO or DENIS wavelength have a very large probability to be real. But sources found only in a 6″ pixel observation, with counterparts neither in the overlapping 3″ pixel observation nor at other wavelengths (or with a bad quality association) may be spurious.

From the available set of overlapping 3″ and 6″ observations, we have determined that the overall fraction of such doubtful sources is very small (∼7%), with a large difference between the 7 $\mu$m (∼4%) and the 15 $\mu$m (∼11%) sources. This fraction also strongly depends on the quality of the sources, and ranges from less than 1% (at both wavelengths) for sources with quality flags $Q = 4$, to ∼15% (resp. ∼30%) for sources with $Q = 1$ or 2 or with $MESH = 1$ or 2 at 7 $\mu$m (resp. at 15 $\mu$m). Therefore sources with quality flags less than 3 should be considered with extreme caution, especially at 15 $\mu$m.

## *3.6. 7–15 $\mu$m cross-identification*

### 3.6.1. Astrometric correction

The initial astrometric accuracy of the ISOCAM data is limited by the errors in the pointing of the telescope and in the positioning of the lens wheels. The global astrometric uncertainty can reach ∼10″ (Blommaert et al. 2001, see also Ott 2002), and the offset between two independent observations can reach twice this value. Therefore an offset correction between the 7 $\mu$m and the 15 $\mu$m observations was needed before the two catalogues could be cross identified. The found offsets are typically of order a few arcseconds, but can reach 15″, in agreement with expectations.

In addition, there can be a small error in the positioning of the individual images within the final raster, due to a combination of possible long term drifts and the lens wheel jitter. Only very small amplitude "distortion" effects have been observed, but a low order polynomial correction was systematically applied to the 15 $\mu$m coordinates to best match the 7 $\mu$m ones.

### 3.6.2. Source associations

After the 15 $\mu$m coordinates were corrected to match those at 7 $\mu$m, an association between 7 $\mu$m and 15 $\mu$m sources was performed with a search radius equal to two pixels. This rather large radius was chosen in order not to miss 7–15 $\mu$m associations for slightly extended sources, and because the density of 15 $\mu$m sources is low enough to limit the probability of chance associations to a few percent in most cases. Only associations with the smallest separation are retained. The mean values of the 7–15 $\mu$m separations are typically in the range 1–3″ in all ISOGAL FC fields, with standard deviations in the same range, as shown in Fig. 5. At the end of this step, the catalogued source coordinates are the most accurate available, namely the 7 $\mu$m coordinates for the sources detected at 7 $\mu$m, or the 15 $\mu$m coordinates translated to the 7 $\mu$m referential for the 15 $\mu$m sources with no 7 $\mu$m association in the FC fields. We kept the initial 15 $\mu$m coordinates only for the sources in FB fields without 7 $\mu$m observations.

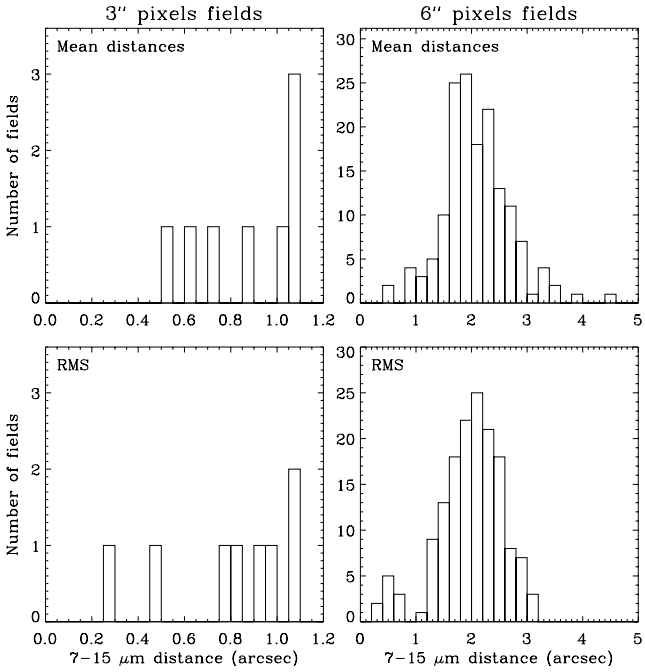


**Fig. 5. Top panel**: distribution of the mean values of the separations between associated 7 $\mu$m and 15 $\mu$m sources after astrometric correction in all ISOGAL FC fields. **Bottom panel**: distribution of the standard deviations of these separations.

### 3.6.3. The 7–15 $\mu$m association quality flag

Finally, a 7–15 $\mu$m association quality flag is computed for each associated source. The value of this flag is defined as follows:

4: the separation between the 7 $\mu$m and the 15 $\mu$m sources is ≤1 pixel and there is only one possible association within a radius of 2 pixels;
3: the separation is still ≤1 pixel but there is another 15 $\mu$m source at less than 2 pixels;
2: the separation is between 1 and 2 pixels, and there is no other source within a radius of 2 pixels;
1: the separation is between 1 and 2 pixels, and there are at least 2 sources within a radius of 2 pixels.

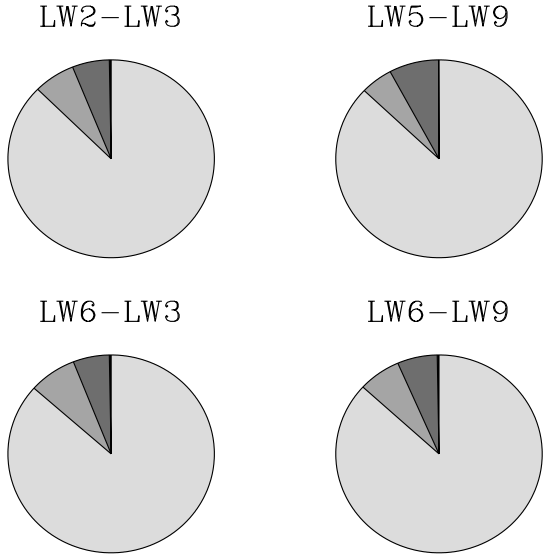


**Fig. 6.** Distribution of the values of the 7–15 $\mu$m association quality flag for the different combinations of 7 and 15 $\mu$m filters. The gray scale corresponds to the different values of this flag, from 4 (lightest gray) to 1 (darkest gray). Only very few sources have this flag equal to 1, so that the darkest gray is hardly visible in these plots.

The distribution of the values of this flag is shown in Fig. 6. A very large majority of the associated sources have a very good quality of association: 87% of the associations have $Q_{7-15} = 4$ and 6.4% have $Q_{7-15} = 3$. Only ∼6% of these flags are equal to 2 and fewer than 0.3% are equal to 1, corresponding to an association distance larger than one pixel. However, 19% of the sources detected at 15 $\mu$m within the area also observed at 7 $\mu$m have no association, while 47% of the 7 $\mu$m sources in the common area have no 15 $\mu$m counterpart. This large difference is explained by the deeper sensitivity of the 7 $\mu$m observations, as compared to the 15 $\mu$m ones.

## 4. DENIS observations of the central Galaxy

In addition to these mid-infrared wavelengths, all the observations in the southern hemisphere (almost 95% of the total area) have been systematically cross-identified with the DENIS (Epchtein et al. 1994, 1997) data, which provide measurements in the three near infrared bands $I$, $J$ and $K_s$.

### 4.1. The DENIS "Bulge" project (Simon et al., in preparation)

In coordination with the ISOGAL project, dedicated observations with the DENIS instrument on the ESO 1 meter telescope at La Silla have been performed, along the inner Galactic plane, between −30 and +10 degrees in galactic longitude, −2 and +2 degrees in latitude, (±4 degrees in the inner Bulge) using a specific technique (Simon et al. in preparation). The individual images ($12' \times 12'$) were taken in a raster mode, covering typically 3 square degrees. Between +10 and +30 degrees in longitude, regular 30° DENIS strips (see Epchtein et al. 1994) were used, with a special reduction procedure. All the DENIS images which have been used to build the ISOGAL PSC are described in the Table of DENIS Observations, whose format is given in Table 8.

### 4.2. Data processing and accuracy

The source extraction has been made through PSF fitting, using the same extraction code as for ISOCAM images. The PSF is modelled in 9 squares on each $12' \times 12'$ individual image and adjusted with respect to the source position. The derived correlation factor gives an evaluation of the photometric uncertainty of the source extraction. For each band, we preserve only the sources with a correlation factor greater than 0.6. The correlation factors are given for each DENIS source in the ISOGAL PSC (Sect. 5).

The saturation of DENIS detectors occurs around magnitude 10 in $I$, 7.5 in $J$ and 6 in $K_s$, and results in severely underestimated flux densities. Therefore, the brightest DENIS sources have been removed from the catalogue. The absolute photometry results from the zero point derived from standard stars observed through the night. A mean value is applied. These magnitudes can be converted to flux densities using the zero points given in Table 9 (from Fouqué et al. 2000).

The limiting sensitivity is about 0.05 mJy (mag. 19) in $I$, 0.5 mJy (mag. 16) in $J$ and 2.5 mJy (mag. 13.5) in $K_s$ but the extraction can become confusion limited in the dense Galactic environment. The relative accuracy of the photometry is checked through the comparison of the measurements in the overlaps (2′ between adjacent images). The average differences are better than 0.03 mag down to magnitudes 17 in $I$ (standard deviation <0.1 mag), 14 in $J$ and 12 in $K_s$ (standard deviation <0.2 mag), which remains very good given the difficulty inherent to such dense regions.

Finally, an image quality flag has been evaluated from the overlapping regions of each DENIS frame covering the ISOGAL rasters. In each band the standard deviation of magnitude differences over a defined magnitude range is calculated (see Table 10) and we assigned a quality flag ranging from 0 (very bad) to 3 (very good). More than one half of the used images have this flag equal to 3, and less than 20% have a flag equal to 1 or 0.

The astrometry is calculated for each image from the present association between $I$ and the USNO_A2 catalogue. Then, the cross associations of $J$ data over $I$, and of $K_s$ data over $J$ are relatively straightforward since all three images have been observed simultaneously. The resulting relative accuracy is better than 0.2″ (RMS) in $I$ and 0.4″ in $J$ and $K_s$. The derived position for $I$ is kept for $I/J/K_s$ associations, and the $J$ position is given for the $J/K_s$ associated sources. From a comparison made with the TYCHO catalogue in the SgrI field in the Baade's Window, no systematic offset was found. The mean value of the distances was 0.36″, with a 0.19″ standard deviation (Simon et al., in preparation). Altogether the present accuracy of the DENIS coordinates used is thus better than 0.5″. It will be improved in the future since it is greatly limited by the accuracy of the astrometry of the USNO_A2 catalogue.

**Table 8.** Format of DENIS observations ($12' \times 12'$ images) Table (version 1).

| Col. | Name | Format | Units [range] | Description |
|---|---|---|---|---|
| 1 | Name | a7 | | image number |
| 2 | date | a6 | YYMMDD | date of observation |
| 3 | j_day | i4 | | Julian day of observation - 2 450 000 |
| 4 | RA | f8.4 | deg | RA (J2000) of image centre |
| 5 | Dec | f8.4 | deg | Dec (J2000) of image centre |
| 6 | G_lon | f7.3 | deg [−180–+180] | Galactic longitude of image centre |
| 7 | G_lat | f7.3 | deg [−90–+90] | Galactic latitude of image centre |
| 8 | *q_I* | i1 | | quality flag of *I* image |
| 9 | *q_J* | i1 | | quality flag of *J* image |
| 10 | *q_K* | i1 | | quality flag of $K_s$ image |

**Table 9.** Isophotal wavelengths and zero point flux densities for the three DENIS bands.

| Band | $\lambda_{iso}$ ($\mu$m) | $F_\nu$ (Jy) |
|---|---|---|
| *I* | 0.791 | 2499 |
| *J* | 1.228 | 1595 |
| $K_s$ | 2.145 | 665 |

**Table 10.** Definition of the DENIS image quality flags.

| | Mag. range | Sigma range | | | |
|---|---|---|---|---|---|
| Flag | | 0 | 1 | 2 | 3 |
| *I* | 11–16 | >0.15 | 0.1–0.15 | 0.07–0.1 | <0.07 |
| *J* | 9–14 | >0.20 | 0.16–0.20 | 0.13–0.16 | <0.13 |
| $K_s$ | 7–12 | >0.20 | 0.16–0.20 | 0.13–0.16 | <0.13 |

### *4.3. ISOGAL–DENIS cross-identification*

The general method that we used to associate DENIS sources with ISOGAL sources is similar to the procedure we used to associate 7 $\mu$m and 15 $\mu$m data. The only difference arises from the very high density of DENIS sources, so that we used a much smaller association radius, and we cut out the faintest DENIS sources when the source density was too high, in order to reduce the probability of chance associations.

#### 4.3.1. Astrometric correction

As explained in Sect. 4.2, the absolute accuracy of the DENIS coordinates is better than 0.5″, thus much better than the ISO astrometry. Therefore we took the DENIS coordinates as the reference system, and computed the global translation offset between the ISOGAL and the DENIS catalogues with the same procedure as for the 7–15 $\mu$m associations. The resulting offsets are typically in the range 3–9″, and can be explained by the lens wheel jitter of ISOCAM (Sect. 3.6.1). This also implies that the coordinates of ISOGAL sources outside the region with DENIS observations can be wrong by this range of distances. An approximate polynomial distortion correction was computed with the same procedure as for the 7–15 $\mu$m associations, in order to match as best as possible the previous ISO reference coordinates with the DENIS ones. Again, the observed effects were of very small amplitude, but this correction was required to correct for small rotations in the ISOCAM rasters.

#### 4.3.2. Confusion cut of weak DENIS sources

The catalogue of DENIS sources covering each ISOGAL field was first limited to sources with a $K_s$ detection, since a $J$–7 $\mu$m association without $K_s$ counterpart has a large probability of being a misidentification. The density remains very high at this stage, exceeding $10^5$ sources/deg$^2$ in the Galactic Centre region. Therefore we further cut the DENIS catalogue to a $K_s$ magnitude that gave a source density of 72 000 sources/deg$^2$ for the ISO 3″ pixel observations. For the observations with 6″ pixels, we proceeded in two steps, first limiting the DENIS source density to 18 000 sources/deg$^2$ and then to 36 000 sources/deg$^2$ (see below). This confusion cut, with the procedure described below, enabled us to limit the probability of chance associations to a few percent even in the most crowded fields.

#### 4.3.3. Source associations

The search for DENIS associations was done with the same procedure as for the 7–15 $\mu$m associations, with a smaller search radius. The mean values of ISO–DENIS separations that we found are typically in the 1–2″ range for all ISOGAL fields, with a few larger values for the FB fields, in which the association is done between DENIS and 15 $\mu$m coordinates (see e.g. Fig. E-31 in the electronic version of this paper). The corresponding standard deviations are mainly in the 1–1.5″ range. An association radius of ~3–4″ is thus appropriate to find most good associations with a low probability of spurious results. However, a close inspection of the distribution of association radii shows that, in a few fields with poor data quality, a few real associations may have a larger association radius, in particular for blended or extended sources with 6″ pixels. Therefore, for the ISO 3″/pixel observations, we used a 3.6″ search radius. But for the ISO 6″/pixel observations, we pushed the search up to a radius of 7″; however, we carefully distinguished by

quality flags the associations with separations smaller or larger than 3.5″.

With such values, the probabilities of random associations may appear high. However, as discussed below, because of the large fraction of real associations with smaller separation, the actual fraction of spurious associations with reasonably good quality flags remains lower than a few percent. The chance of spurious association is larger for weaker $K_s$ sources allowed with the higher density limit. The final ISO–DENIS quality flag (Sect. 4.3.4) takes this point into account.

#### 4.3.4. The ISO–DENIS association flag

The ISO–DENIS association is characterised by a specific quality flag, $Q_{ID}$, which ranges in values from 5 (highest quality) to 0 (no association). The computation of this flag takes into account:

- the separation between the ISO source and the associated closest DENIS source;
- the number of DENIS sources within the search radius;
- the global quality of ISO–DENIS associations for each field, as derived from a visual inspection of the histograms of the distances of associations;
- for the ISO 6″ observations only, the value of this flag is decreased for sources with a $K_s$ magnitude between the two cutoff magnitudes $K$_max1 and $K$_max2 (Cols. 16 and 17 of the table of ISOGAL fields, see Table 4), which were used to limit the source density of the DENIS catalogue to 18 000 and 36 000 sources per square degree, respectively.

Let us stress the large fraction of DENIS associations, ∼92% for 7 $\mu$m sources, ∼79% for 15 $\mu$m sources in FB fields and ∼45% for 15 $\mu$m sources with no 7 $\mu$m association in FC fields (Fig. 7). The fraction of associations with $K$_max1 < $K_s$ < $K$_max2 is also small, ∼4% for 7 $\mu$m sources, ∼2.5% for 15 $\mu$m sources in FB fields and ∼17% for 15 $\mu$m sources with no 7 $\mu$m association in FC fields. Therefore, the fraction of spurious associations among accepted associations (see below) always remains small, typically at most ∼1% for 7 $\mu$m sources and a few percent for 15 $\mu$m sources.

Finally when the derivation leads to $Q_{ID} = 0$, the association is considered as invalid and no DENIS association is given in the catalogue. With this definition, associations with a quality flag equal to 4 or 5 can be considered as secure, while a value of 3 is more uncertain but remains a high probability association, and values of 1 or 2 are more doubtful but still include an appreciable fraction of real associations. The distribution of the computed ISO–DENIS association flags is shown in Fig. 7, where it can be seen that ∼87% of the associations found have a good quality (flag ≥ 4), while fewer than 8% of the 7 $\mu$m sources (LW2, LW5 and LW6 filters) within the area observed by DENIS have no association.

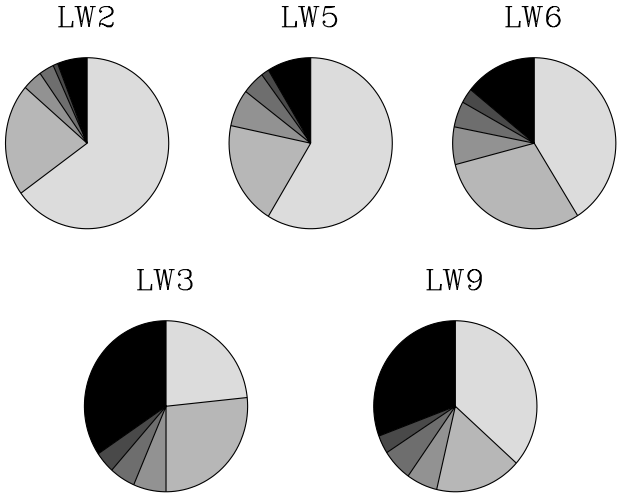


**Fig. 7.** Distributions of the ISO–DENIS association flag for the different ISO filters. The gray scale corresponds to the different values of this flag, from 5 (lightest gray) to 1 (darkest gray), and the black sectors show the fraction of sources without DENIS association within the area observed by DENIS.

## 5. ISOGAL–DENIS Point Source Catalogue (version 1)

The Point Source Catalogue contains a total of 106 150 sources, and is composed of two sections. For each field, the "regular" catalogue contains all the sources inside the formal limits of the rectangular field, as defined in Table 4 (see example in Fig. 1). These limits have been computed to avoid any border effects: all the sources inside this area are located at more than two pixels from the saw-tooth edges of the observed raster, both at 7 and 15 $\mu$m for FC fields. This differs from the EDGE flag computed for each wavelength (see Sect. 3.2.3) since the "regular" region is limited to a rectangular area (whose axis are aligned along the galactic ones) which has been fully observed at both wavelengths.

Then, the "edge" catalogue contains the sources outside the limits of the rectangular field, but excluding the measurements at less than two pixels from the saw-tooth edges. This means that in the "edge" region of an FC field, it is possible to find a source with for example a 7 $\mu$m detection and no 15 $\mu$m counterpart, simply because the edges of the 15 $\mu$m raster do not exactly match the ones of the 7 $\mu$m raster, so that the source can be outside the region observed at 15 $\mu$m or within 2 pixels of one saw-tooth edge. As a result, ∼53% of the 7 $\mu$m sources and ∼81% of the 15 $\mu$m sources in the "regular" regions of all FC fields have an association at the other ISO wavelength, while these fractions become ∼47% for 7 $\mu$m sources and ∼70% for 15 $\mu$m sources in the "edge" regions.

Both the "regular" and the "edge" catalogues have the format described in Table 11, and a few examples of entries are given in Table 12. The final Catalogue contains 93 385 sources in the "regular" regions, and 12 765 sources in the "edge" regions.

### *5.1. Position data*

The first ten entries for each source in the PSC consist of general data, as described below.

- Column 1: source number in the field. This number increases with the right ascension of the sources.

Each individual catalogue (the "regular" and the "edge" for each field) contains its own numbering, and these numbers are preceded by an "E" in the "edge" catalogues.

– Column 2: source name. It is composed of 25 characters, following the format:

  ISOGAL − P*Jhhmmss.s* ± *ddmmssX*

  where "ISOGAL" stands for the ISOGAL–DENIS data, the "P" means that these are provisory data, and the *Jhhmmss.s* ± *ddmmss* are the J2000 equatorial coordinates of the source, as they appear in Cols. 3 and 4. The last character, "*X*", is left blank in all cases but those where two (or exceptionally three) sources from different fields are found at the same position, because they are associated with the same DENIS source and because of edge effects. This concerns 842 sources (0.8% of the PSC) and in all those cases, at least one of the coinciding sources is in an "edge" catalogue. A letter is appended to the name of the sources, starting with an *a* for that in a "regular" catalogue if it exists, otherwise using an arbitrary order between the "edge" catalogues, and going to *b* or *c* when needed.
– Columns 3 and 4: reference J2000 equatorial coordinates, expressed in decimal degrees (see the footnote *b* in Table 11).
– Columns 5 and 6 give the ISOGAL corrected coordinates, which are the ISOGAL extracted coordinates when there is no DENIS observation of the field, or the ISOGAL corrected to DENIS system ones when a DENIS observation exists.
– Columns 7 and 8 give the galactic reference coordinates corresponding to the reference coordinates given in Cols. 3 and 4, in the commonly used ($l^{II}$, $b^{II}$) galactic system.
– Column 9 gives the name of the ISOGAL field.
– Column 10 gives the last seven digits of the number of the DENIS image where an ISO–DENIS association was found. For ISOGAL sources with no DENIS counterpart, this column contains 0000000.

### 5.2. DENIS data

All the DENIS data are given in Cols. 11 to 22. For each of the three bands, these data are the measured magnitude, the correlation factor with the PSF, and the pixel coordinates of the source in the individual DENIS 12′ × 12′ image, whose reference number is given in Col. 10.

For the ISOGAL sources within the area observed by DENIS but with no DENIS association, the $I$, $J$ and $K_s$ magnitudes are set to 99.99, while they are set to 88.88 for all the sources located outside the region surveyed by DENIS. In these two cases, the PSF correlation factors and pixel coordinates are set to 0.

The correlation factors with the PSF give an indication of the photometric quality (see Simon et al., in preparation): the uncertainty on the measured magnitude is small when this factor is ≥0.95. On the other hand, a value ≤0.85 means that the photometry is more uncertain (typically by 0.1 to 0.2 mag). For bright sources, this may come from moderate saturation effects, while for faint sources, a value ≤0.80 is more typical. Nevertheless, a factor ≤0.70 indicates a poor photometric quality, which may be caused by blending effects or confusion with the background.

### 5.3. ISOCAM data

Columns 23 to 42 give all the data derived from individual 7 and 15 $\mu$m ISO observations, including quality flags (see Sect. 3.2.3), calibrated magnitudes, uncertainties ($\sigma$) from the PSF fit measurement of the magnitudes, pixel positions in the final image (after correction of the orientation, see Sect. 7), filter numbers and pixel sizes.

### 5.4. Association quality flags

The value of the ISOGAL 7–15 $\mu$m association flag (see definition in Sect. 3.6.3) is given in Col. 44, and the separation (in arcseconds) between the 7 $\mu$m and the 15 $\mu$m positions (after correction of the field offset) is given in Col. 43. This flag and the corresponding separation are set to zero for sources with no 7–15 $\mu$m association.

For the ISO–DENIS association, the quality flag (see definition in Sect. 4.3.4) is given in Col. 46, and the separation (in arcseconds) between the ISO and the DENIS positions (after correction of the field offset) is given in Col. 45. Again, these two entries are set to zero when there is no ISO–DENIS association.

### 5.5. Examples

Table 12 shows three examples of entries in the ISOGAL–DENIS Point Source Catalogue. These sources are located in the "C32" field ($l$ = 0.0, $b$ = +1.0). The first one has been detected at 7 $\mu$m but not at 15 $\mu$m, and has a DENIS association. The second one has been detected at 7 and 15 $\mu$m but has no DENIS association. Finally, the third one is detected in all five bands.

## 6. Catalogue of spurious sources

As explained in Sect. 3.2.5, three kinds of extracted sources brighter than the limiting magnitude of each field are considered spurious: (1) the sources found only in the "inversion" processed raster, with no counterpart in a 1 pixel search radius in the "vision" raster, (2) the sources with simultaneously a doubtful inversion-vision association (with a separation between 0.5 and 1 pixel) and with a poor detection confirmation (i.e. with no association between the *mesh* = 1 and the *mesh* = 2 results), and (3) the possible remnants of bright sources, found by a procedure that looked at the same pixel location in the five successive images of the implied raster.

These sources are published in three distinct tables. Their format is defined in Table 13. The numbers, as they appear in Col. 1, are preceded by an "I" for the "inversion-only" sources, by an "M" for the sources of the second class and by an "R" for the probable remnants.

Note that most spurious sources of the first two kinds are probably artifacts, but can also be related to faint extended

**Table 11.** Format of the ISOGAL Point Source Catalogue (version 1) – 106 150 entries (see examples in Table 12).

| Col. | Name | Format | Units [range] | Description |
|---|---|---|---|---|
| 1 | Number | a5 | | source identification number in the field |
| 2 | Name | a25 | ISOGAL-PJ*hhmmss.s* ± *ddmmssX* | source identifier (J2000)[a] |
| 3 | RAJ2000 | f8.4 | deg [0–360] | Right Ascension (J2000)[b] |
| 4 | DEJ2000 | f8.4 | deg [−90–+90] | Declination (J2000) |
| 5 | RAISOGAL | f8.4 | deg [0–360] | ISOGAL RA (J2000) |
| 6 | DEISOGAL | f8.4 | deg [−90–+90] | ISOGAL Dec (J2000) |
| 7 | G_lon | f8.4 | deg [−180–+180] | Galactic longitude |
| 8 | G_lat | f8.4 | deg [−90–+90] | Galactic latitude |
| 9 | I_field | a14 | Fxsllllsbbbbb | ISOGAL field name |
| 10 | D_field | a7 | | DENIS image name[c] |
| 11 | *I*mag | f5.2 | mag | DENIS *I*-band magnitude[d] |
| 12 | *I*corr | f4.2 | [0–1] | DENIS *I*-band correlation factor |
| 13 | *x_I* | f5.1 | pixel | *x*-position in DENIS *I*-band image |
| 14 | *y_I* | f5.1 | pixel | *y*-position in DENIS *I*-band image |
| 15 | Jmag | f5.2 | mag | DENIS *J*-band magnitude[d] |
| 16 | Jcorr | f4.2 | [0–1] | DENIS *J*-band correlation factor |
| 17 | *x_J* | f5.1 | pixel | *x*-position in DENIS *J*-band image |
| 18 | *y_J* | f5.1 | pixel | *y*-position in DENIS *J*-band image |
| 19 | *K*mag | f5.2 | mag | DENIS $K_s$-band magnitude[d] |
| 20 | *K*corr | f4.2 | [0–1] | DENIS $K_s$-band correlation factor |
| 21 | *x_K* | f5.1 | pixel | *x*-position in DENIS $K_s$-band image |
| 22 | *y_K* | f5.1 | pixel | *y*-position in DENIS $K_s$-band image |
| 23 | mag7 | f5.2 | mag | ISOGAL 7 $\mu$m magnitude[d] |
| 24 | e_mag7 | f4.2 | mag | uncertainty in 7 $\mu$m magnitude |
| 25 | filt_7 | i1 | [2,5,6] | LW number of filter used |
| 26 | pfov_7 | i1 | arcsec [3,6] | pixel field of view |
| 27 | *x_7* | f6.2 | pixel | *x*-position on ISOGAL final 7 $\mu$m image |
| 28 | *y_7* | f6.2 | pixel | *y*-position on ISOGAL final 7 $\mu$m image |
| 29 | npix_7 | i1 | [0–7] | npix flag at 7 $\mu$m (see Sect. 3.2.3) |
| 30 | mesh_7 | i1 | [1,2,3] | mesh flag at 7 $\mu$m (see Sect. 3.2.3) |
| 31 | edge_7 | i1 | [0,1] | edge flag at 7 $\mu$m (see Sect. 3.2.3) |
| 32 | qual_7 | i1 | [0–4] | global quality flag at 7 $\mu$m (see Sect. 3.2.3) |
| 33 | mag15 | f5.2 | mag | ISOGAL 15 $\mu$m magnitude[d] |
| 34 | e_mag15 | f4.2 | mag | uncertainty in 15 $\mu$m magnitude |
| 35 | filt_15 | i1 | [3,9] | LW number of filter used |
| 36 | pfov_15 | i1 | arcsec [3,6] | pixel field of view |
| 37 | *x_*15 | f6.2 | pixel | *x*-position on ISOGAL final 15 $\mu$m image |
| 38 | *y_*15 | f6.2 | pixel | *y*-position on ISOGAL final 15 $\mu$m image |
| 39 | npix_15 | i1 | [0–7] | npix flag at 15 $\mu$m (see Sect. 3.2.3) |
| 40 | mesh_15 | i1 | [1,2,3] | mesh flag at 15 $\mu$m (see Sect. 3.2.3) |
| 41 | edge_15 | i1 | [0,1] | edge flag at 15 $\mu$m (see Sect. 3.2.3) |
| 42 | qual_15 | i1 | [0–4] | global quality flag at 15 $\mu$m (see Sect. 3.2.3) |
| 43 | dis_II | f5.2 | arcsec | separation 7 to 15 $\mu$m associated sources |
| 44 | ass_II | i1 | [0–4] | 7–15 $\mu$m association quality flag |
| 45 | dis_ID | f5.2 | arcsec | separation ISOGAL to DENIS associated sources |
| 46 | ass_ID | i1 | [0–5] | ISOGAL–DENIS association quality flag |

[a] The last character "*X*" is only present when two sources with the same position have to be distinguished (see text, Sect. 5.1).
[b] Coordinates: the final adopted coordinates (Cols. 3 and 4) are the DENIS ones if there is an association, or the ISO corrected to DENIS if an observation exists but no source was associated. In the northern fields (without DENIS), the coordinates are the 7 $\mu$m ones if they exist, or the 15 $\mu$m ones for the sources in FB fields, and the 15 $\mu$m corrected to 7 $\mu$m for the sources detected only at 15 $\mu$m in the FC fields. When no DENIS association exists, RAJ2000 = RAISOGAL and DEJ2000 = DEISOGAL.
[c] Only the seven last digits of the DENIS numbers have been stored, as the three first ones are always 000.
[d] A value of 88.88 for a magnitude means that this position was not observed at this wavelength, while a value of 99.99 means that the source was not detected at this wavelength.

**Table 12.** Examples of entries in the ISOGAL–DENIS Point Source Catalogue from the C32 field.

| Col. | Name | Example 1 | Example 2 | Example 3 |
|---|---|---|---|---|
| 1 | Number | 0008 | 0017 | 0007 |
| 2 | Name | ISOGAL-PJ174118.0-282916 | ISOGAL-PJ174122.7-283146 | ISOGAL-PJ174117.6-282901 |
| 3 | RAJ2000 | 265.3250 | 265.3446 | 265.3234 |
| 4 | DEJ2000 | −28.4880 | −28.5296 | −28.4838 |
| 5 | RAISOGAL | 265.3251 | 265.3446 | 265.3230 |
| 6 | DEISOGAL | −28.4880 | −28.5296 | −28.4837 |
| 7 | G_lon | −0.1158 | −0.1419 | −0.1129 |
| 8 | G_lat | 1.0415 | 1.0048 | 1.0449 |
| 9 | I_field | FC+00000+00100 | FC+00000+00100 | FC+00000+00100 |
| 10 | D_field | 0955338 | 0000000 | 0955339 |
| 11 | *I*mag | 16.49 | 99.99 | 16.36 |
| 12 | *I*corr | 0.96 | 0.0 | 0.91 |
| 13 | *x_I* | 367.7 | 0.0 | 376.6 |
| 14 | *y_I* | 153.8 | 0.0 | 735.6 |
| 15 | Jmag | 10.87 | 99.99 | 10.63 |
| 16 | Jcorr | 0.99 | 0.0 | 0.98 |
| 17 | *x_J* | 369.9 | 0.0 | 371.1 |
| 18 | *y_J* | 154.9 | 0.0 | 745.1 |
| 19 | *K*mag | 8.32 | 99.99 | 8.02 |
| 20 | *K*corr | 0.98 | 0.0 | 0.99 |
| 21 | *x_K* | 368.1 | 0.0 | 370.5 |
| 22 | *y_K* | 151.8 | 0.0 | 750.9 |
| 23 | mag7 | 7.60 | 3.47 | 7.36 |
| 24 | e_mag7 | 0.03 | 0.01 | 0.03 |
| 25 | filt_7 | 2 | 2 | 2 |
| 26 | pfov_7 | 6 | 6 | 6 |
| 27 | *x_7* | 165.76 | 181.81 | 164.10 |
| 28 | *y_7* | 71.76 | 50.07 | 74.02 |
| 29 | npix_7 | 2 | 0 | 2 |
| 30 | mesh_7 | 3 | 3 | 3 |
| 31 | edge_7 | 0 | 0 | 0 |
| 32 | qual_7 | 4 | 4 | 4 |
| 33 | mag15 | 99.99 | 1.54 | 5.84 |
| 34 | e_mag15 | 0.00 | 0.03 | 0.06 |
| 35 | filt_15 | 0 | 3 | 3 |
| 36 | pfov_15 | 0 | 6 | 6 |
| 37 | *x_15* | 0.00 | 181.64 | 163.77 |
| 38 | *y_15* | 0.00 | 49.86 | 73.49 |
| 39 | npix_15 | 0 | 1 | 2 |
| 40 | mesh_15 | 0 | 3 | 3 |
| 41 | edge_15 | 0 | 0 | 0 |
| 42 | qual_15 | 0 | 4 | 4 |
| 43 | dis_II | 0.00 | 1.06 | 1.16 |
| 44 | ass_II | 0 | 4 | 4 |
| 45 | dis_ID | 0.32 | 0.00 | 1.25 |
| 46 | ass_ID | 5 | 0 | 5 |

structures, for which different parameters in the extraction process result in slightly different coordinates. The third class of spurious sources is essentially composed of spurious remnants, but may contain a few real sources, which have been accidentally discarded by the procedure because of spatial coincidence with a putative remnant.

## 7. ISOCAM corrected images

The ISOCAM images have been initially processed using version 7.0 of the off-line processing pipeline (Sect. 3.1). Similar images processed with the latest version of OLP are now publically available through the Data Archive on the ISO web site[5]. However, we make available here the OLP7 images together with version 1 of the PSC for consistency, because they have been used for the extraction of the sources of this catalogue. Improved ISOGAL images (Miville-Deschênes et al. 2000 and in preparation) will be published with version 2 of the catalogue.

[5] `http://www.iso.vilspa.esa.es/ida/index.html`

Because of the difference in orientation between the individual images (aligned along the satellite axis, thus with the equatorial coordinates) and the mosaiced rasters (aligned along the galactic axes), and of different times of observations, the orientation obtained after the OLP7 processing was different from one raster to another. We therefore decided to change this orientation if necessary, in order to use the same convention for all rasters, and set the orientation to $l$ along decreasing $X$ and $b$ along increasing $Y$.

A more important improvement provided by the construction of the ISOGAL PSC deals with the astrometry, which has been tied to DENIS whenever possible. The offsets that we applied to the source coordinates in order to associate the ISO sources with DENIS have also been applied to the rasters, as indicated in Table 2. For the FC fields with no DENIS observation, the astrometry of the 15 $\mu$m rasters has been tied to that of the 7 $\mu$m ones. The corrected images are available through the CDS and the IAP[6] server.

## 8. Summary

The first version of the ISOGAL–DENIS Point Source Catalogue contains a total of 106 000 sources, with one or two magnitude measurements in the mid-infrared (7 and 15 $\mu$m), and up to three magnitude measurements in the near-infrared ($I$, $J$ and $K_s$ bands of the DENIS survey, see Tables 11 and 12). The data are presented in two similar tables, corresponding to the "regular" and the "edge" regions of the observed fields. The latter contains the sources from the edges of the ISOCAM rasters, where border effects can occur, which can lead to non-association between the two ISO bands.

The typical RMS photometric uncertainty is at most ∼0.1 mag for the DENIS bands, and better than 0.15 mag for the ISO bands in most cases, but it can reach 0.3 mag for the faintest sources in the densest fields. For the most numerous fields observed with broad filters, the limiting magnitudes of the published catalogues range between 8.8 and 10.1 at 7 $\mu$m (with a median value equal to 9.46 mag, or $F_\nu \sim 15$ mJy), and between 7.7 and 8.8 at 15 $\mu$m (median 8.16 mag, $F_\nu \sim 11$ mJy), depending on the source density. For the most difficult fields observed with narrow filters, these limits range between 8.2 and 9.6 mag at 7 $\mu$m and between 7.0 and 8.2 mag at 15 $\mu$m. These limits are conservative and the fainter sources have been rejected in the present version of the PSC[7].

The current astrometric accuracy of the DENIS data used is better than 0.5″ (RMS). The final coordinates (as they appear in Cols. 3 and 4 of the catalogue – see Table 11 – in equatorial J2000 system, in Cols. 7 and 8 in the galactic system, and in the name of the source, Col. 2) of all ISOGAL sources with a DENIS counterpart are the DENIS ones, and should also be accurate to 0.5″. The astrometry of the ISOGAL sources with no DENIS association, but within the fields observed by DENIS, is also tied to the DENIS coordinates, and should therefore be accurate to ∼2″ (RMS). Finally, ISOGAL sources located outside the area surveyed by DENIS may suffer from the lens wheel jitter of ISOCAM, resulting in a maximum ∼10″ systematic offset in the extracted coordinates.

Several flags have been implemented to characterise the reliability of the sources, the quality of their photometry and of the associations between the different bands. An indication of the reliability of the mid-infrared detection is also given by the *mesh* flag (Col. 30 for 7 $\mu$m and Col. 40 for 15 $\mu$m, see Table 11). A value of 3 indicates a good reliability level, while a value of 1 or 2 shows that the extraction was not perfectly confirmed, making the real point-like nature of the source doubtful.

The global quality of the ISO photometry and reliability of each source is quantified by one quality flag for each band. These two flags are given in Col. 32 for 7 $\mu$m and in Col. 42 for 15 $\mu$m, and range from 1 to 4, the highest value corresponding to the best quality. Thus sources with quality flags equal to 1 or 2 should be considered with caution.

The quality of the association between the two ISO bands is also characterised by a specific flag, which appears in Col. 44, together with the separation of the association in Col. 43. When this flag is equal to 3 or 4, which means that the separation between the 7 $\mu$m coordinates and the 15 $\mu$m ones is smaller than one pixel, the validity of the association is almost certain, while a value of 1 or 2 means that the association has to be carefully checked, but it may be a real association for slightly extended sources.

Finally, the quality of the ISO–DENIS association is quantified by a flag given in Col. 46 (and the ISO–DENIS separation appears in Col. 45). Here, values of 4 or 5 correspond to secure associations, while a value of 3 means that the association was not straightforward, but it still has a good probability to be real. When this flag is equal to 1 or 2, the reality of the association has to be checked carefully, using for instance colour compatibility criteria.

## 9. Conclusion

With the first public version of the ISOGAL–DENIS Point Source Catalogue, we provide the astronomical community with a catalogue containing about $10^5$ mid-infrared sources, detected at 7 and/or 15 $\mu$m in the obscured centre of the Galaxy. The bulk of them are associated with near-infrared data from the DENIS survey. We also provide nearly 400 mid-infrared images, with an astrometric accuracy of ∼1″ for most of them.

All the data were reduced using data products of version 7 of the ISO off-line processing pipeline. Additional specific procedures enabled us to greatly reduce the number of artifacts and to reduce the photometric uncertainty to typically 0.15 mag, at the cost of limiting the published catalogue in the densest observed fields to levels well above the sensitivity limit of a few mJy.

A second version of the catalogue is already under development, based on a systematic reprocessing of the raw data using the most up-to-date specialised procedures (Miville-Deschênes 2000 and in preparation). This second version will also contain systematic cross-associations with the near-infrared data

[6] http://www-isogal.iap.fr/Fields/index_tdt.html

[7] The complete catalogues, including the faint sources rejected, may be obtained by requesting the ISOGAL PI, omont@iap.fr

**Table 13.** Format of spurious sources Table (version 1).

| Col. | Name | Format | Units [range] | Description |
|---|---|---|---|---|
| 1 | Number | a4 | | identification number in the ION |
| 2 | RAJ2000 | f8.4 | deg [0–360] | ISOGAL RA (J2000) |
| 3 | DEJ2000 | f8.4 | deg [−90–+90] | ISOGAL Dec (J2000) |
| 4 | Mag | f5.2 | mag | ISOGAL magnitude |
| 5 | ION | a8 | | ISO observation number |
| 6 | *x* | f6.2 | pixel | *x*-position on ISOGAL final image |
| 7 | *y* | f6.2 | pixel | *y*-position on ISOGAL final image |

of the 2MASS survey, and with the mid-infrared data of the MSX survey.

*Acknowledgements.* We thank the whole ISOGAL Team for its contribution to the project and to the production of the present catalogue.

The ISOCAM data presented in this paper were analysed using "CIA", a joint development by the ESA Astrophysics Division and the ISOCAM Consortium. The ISOCAM Consortium is led by the ISOCAM PI, C. Cesarsky. We thank A. Abergel, H. Aussel, A. Coulais, R. Gastaud, M. Pérault, J. L. Starck and many other members of the ISOCAM team, of the ISO/ESA team at Villafranca and especially of the CIA team for their help in the ISOGAL data reduction. We are very grateful to all people who contributed to the ISOGAL data reduction, including T. August, X. Bertou, E. Copet and M. Unavane.

We thank the whole DENIS Team, and especially its PI, N. Epchtein, and S. Bégon, J. Borsenberger, B. de Batz, P. Fouqué, S. Kineswenger & D. Thiphène for making available the DENIS data. The DENIS project is supported, in France by the Institut National des Sciences de l'Univers, the Education Ministry and the Centre National de la Recherche Scientifique, in Germany by the State of Baden-Würtemberg, in Spain by the DGICYT, in Italy by the Consiglio Nazionale delle Ricerche, in Austria by the Fonds zur Förderung der wissenschaflichen Forschung and the Bundesministerium für Wissenschaft und Forschung.

This publication made use of data products from the Midcourse Space Experiment. Processing of the data was funded by the Ballistic Missile Defense Organization with additional support from NASA Office of Space Science.

This work was carried out in the context of EARA, the European Association for Research in Astronomy.

S. Ganesh was supported by a fellowship from the Ministère des Affaires Étrangères, France, and this research was supported by the Project 1910-1 of Indo-French Center for the Promotion of Advanced Research (CEFIPRA). SG also acknowledges the support he received from the French CNRS for participating in the astronomical school in Les Houches in 1998. M. Schultheis acknowledges the receipt of an ESA fellowship. B. Aracil and A. Soive were posted to the ISOGAL Project by the Délegation Générale de l'Armement, France.

We are grateful to Dr. M. Cohen for his help in the calibration of ISOCAM data, and to Dr. S. Ott and Prof. I. S. Glass for their useful comments and inputs.

## References

Abergel, A., Miville-Deschênes, M.-A., Désert, F.-X., et al. 1998, The transient behaviour of the long wavelength channel of ISOCAM, http://www.iso.vilspa.esa.es/users/expl_lib/CAM/transient_detector_ws.ps.gz

Aussel, H. 1998, August 13, ISOCAM LW channel Field of View Distortion, http://www.iso.vilspa.esa.es/users/expl_lib/CAM/distortion.ps.gz

Bellazzini, M., Fusi Pecci, F., Montegriffo, P., et al. 2002, AJ, 123, 2541

Biviano, A., Sauvage, M., Gallais, P., et al. 1998, May 18, The ISOCAM Dark Current Calibration Report, http://www.iso.vilspa.esa.es/users/expl_lib/CAM/darkdoc.ps.gz

Blommaert, J. A. D. L. 1998, December 18, ISOCAM Photometry Report, http://www.iso.vilspa.esa.es/users/expl_lib/CAM/photom_rep_fn.ps.gz

Blommaert, J. A. D. L., Metcalfe, L., Altieri, B., et al. 2000, Exp. Astron., 10, 241

Blommaert, J. A. D. L., Siebenmorgen, R., Coulais, A., et al. 2001, The ISO Handbook, Volume III: CAM - The ISO Camera, http://www.iso.vilspa.esa.es/manuals/HANDBOOK/III/cam_hb/

Bontemps, S., André, P., Kaas, A. A., et al. 2001, A&A, 372, 173

Burgdorf, M. J., Cohen, M., Price, S. D., et al. 2000, A&A, 360, 111

Cesarsky, C. J., Abergel, A., Agnèse, P., et al. 1996, A&A, 315, L32

Coulais, A., & Abergel, A. 2000, A&AS, 141, 533

Dole, H., Gispert, R., Lagache, G., et al. 2001, A&A, 372, 364

Egan, M. P., Shipman, R. F., Price, S. D., et al. 1998, ApJ, 494, L199

Elbaz, D., Cesarsky, C. J., Fadda, D., et al. 1999, A&A, 351, 37

Epchtein, N., de Batz, B., Copet, E., et al. 1994, Ap&SS, 217, 3

Epchtein, N., de Batz, B., Capoani, L., et al. 1997, The Messenger, 87, 27

Felli, M., Comoretto, G., Testi, L., Omont, A., & Schuller, F. 2000, A&A, 362, 199

Felli, M., Testi, L., Schuller, F., & Omont, A. 2002, A&A, 392, 971

Fouqué, P., Chevallier, L., Cohen, M., et al. 2000, A&AS, 141, 313

Glass, I. S., Ganesh, S., Alard, C., et al. 1999, MNRAS, 308, 127

Hammersley, P. L., Jourdain de Muizon, M., Kessler, M. F., et al. 1998, A&AS, 128, 207

Hennebelle, P., Pérault, M., Teyssier, D., & Ganesh, S. 2001, A&A, 365, 598

Jiang, B. W., Omont, A., Ganesh, S., Simon, G., & Schuller, F. 2003, A&A, 400, 903

Kessler, M. F., Steinz, J. A., Anderegg, M. E., et al. 1996, A&A, 315, L27

Lumsden, S. L., Hoare, M. G., Oudmaijer, R. D., & Richards, D. 2002, MNRAS, 336, 621

Mill, J. D., O'Neil, R. R., Price, S., et al. 1994, Spacecraft Rockets, 31, 900

Miville-Deschênes, M.-A., Boulanger, F., Abergel, A., & Bernard, J.-P. 2000, A&AS, 146, 519

Nordh, L., Olofsson, G., Bontemps, S., et al. 1998, in Star Formation with the Infrared Space Observatory, ed. J. Yun, & R. Liseau, ASP Conf. Ser., 132, 127

Ojha, D. K., Omont, A., Schuller, F., et al. 2003, A&A, 403, 141

Omont, A., Ganesh, S., Alard, C., et al. 1999, A&A, 348, 755

Omont, A., Gilmore, G. F., Alard, C., et al. 2003, A&A, 403, 975

Ortiz, R., Blommaert, J. A. D. L., Copet, E., et al. 2002, A&A, 388, 279

Ott, S., Abergel, A., Altieri, B., et al. 1997, Design and Implementation of CIA, the ISOCAM Interactive Analysis System. in ed. G. Hunt, & H. E. Payne, ASP Conf. Ser., 125, 34
Ott, S. 2002, Ph.D. Thesis, Paris VI - Pierre et Marie Curie University
Pérault, M., Omont, A., Simon, G., et al. 1996, A&A, 315, L165
Price, S. D., Egan, M. P., Carey, S. J., Mizuno, D. R., & Kuchar, T. A. 2001, AJ, 121, 2819
Rowan-Robinson, M., Oliver, S., Efstathiou, A., et al. 1999, in The Universe as Seen by ISO, ed. P. Cox, & M. F. Kessler, ESA-SP 427, 1011
Schuller, F. 2002, Ph.D. Thesis, Paris VI - Pierre et Marie Curie University
Schultheis, M., Ganesh, S., Glass, I. S., et al. 2000, A&A, 362, 215
Skrutskie, M. F., Schneider, S. E., Stiening, R., et al. 1997, in The Impact of Large Scale Near-IR Sky Surveys, ed. F. Garzon, N. Epchtein, A. Omont, et al. (Dordrecht: Kluwer), 25
Starck, J.-L. 1998, in Les Houches Summer School on Infrared Astronomy from Space: Today and Tomorrow
Starck, J.-L., Murtagh, F., & Bijaoui, A. 1998, Image Processing and Data Analysis: The Multiscale Approach (Cambridge University Press)
Testi, L., Felli, M., Omont, A., et al. 1997, A&A, 318, L13
Zavagno, A., & Ducci, V. 2001, A&A, 371, 312